Sub-millennial climate variability from high resolution water isotopes in the EDC ice core

Antoine Grisart[(1)], Mathieu Casado[(1,3)], Vasileios Gkinis[(2)], Bo Vinther[(2)], Philippe Naveau[(1)], Mathieu Vrac[(1)], Thomas Laepple[(3)], Bénédicte Minster[(1)], Frederic Prié[(1)], Barbara Stenni[(4)], Elise Fourré[(1)], Hans Christian Steen-Larsen[(5)], Jean Jouzel[(1)], Martin Werner[(6)], Katy Pol[(1)], Valérie Masson-Delmotte[(1)], Maria Hoerhold[(6)], Trevor Popp[(2)], Amaelle Landais[(1)]

[1] Laboratoire des Sciences du Climat et de l'Environnement, CEA–CNRS–UVSQ–Paris-Saclay–IPSL, Gif-sur-Yvette, France
[2] Physics of Ice, Climate and Earth, Niels Bohr Institute, University of Copenhagen, Copenhagen, Denmark
[3] Alfred Wegener Institute, Helmholtz Center for Polar and Marine Research, Potsdam, Germany
[4] Department of Environmental Sciences, Informatics and Statistics, University Ca' Foscari of Venice, Venice, Italy
[5] Geophysical Institute, University of Bergen and Bjerknes Centre for Climate Research, Bergen 5020, Norway
[6] Alfred Wegener Institute, Helmholtz Centre for Polar and Marine Research, Bremerhaven, Germany

Correspondence to: Antoine Grisart (antoine.grisart@lsce.ipsl.fr)

Abstract. The EPICA Dome C (EDC) ice core provides the longest continuous climatic record covering the last 800,000 years (800 kyrs). A unique opportunity to investigate decadal to millennial variability during past glacial and interglacial periods is provided by the high resolution water isotopic record ($\delta^{18}O$ and δD) available for the EDC ice core. We present here a continuous compilation of the EDC water isotopic record at a sample resolution of 11 cm which consists of 27,000 $\delta^{18}O$ measurements and 7,920 δD measurements (covering respectively 94 % and 27 % of the whole EDC record), including published and new measurements (2,900 for both $\delta^{18}O$ and δD) over the last 800 kyrs. Here, we demonstrate that repeated water isotope measurements on the same EDC samples from different depth intervals obtained using different analytical methods are comparable within analytical uncertainty. We thus combine all available EDC water isotope measurements to generate a high resolution (11 cm) data set over the past 800 kyrs. A frequency decomposition of the most complete $\delta^{18}O$ record and a simple assessment of the possible influence of diffusion on the measured profile shows that the variability at multi-decadal to multi-centennial timescale is higher during glacial than during interglacial periods, and higher during early interglacial isotopic maxima than during the Holocene. This analysis shows as well that during interglacial periods characterized by a temperature optimum at its beginning, the multi-centennial variability is the strongest over this temperature optimum.

1 Introduction

Water stable isotopes (oxygen, $\delta^{18}O$; and hydrogen, δD) in ice cores are valuable proxy records that can be used to reconstruct past temperatures in polar regions. Water isotopic composition from ice core samples is classically measured with delta notation (δ) expressing the variations of isotopic ratio of heavy to light isotopes in the water molecule (i.e. $^{18}O/^{16}O$ and D/H for $\delta^{18}O$ and δD). Along air mass transportation, distillation of moisture from the low latitude regions of evaporation to the

polar regions leads to a preferential loss of heavy isotopes ($H_2{}^{18}O$ and $HD^{16}O$ vs $H_2{}^{16}O$) during successive precipitation events and hence to a decrease of $\delta^{18}O$ and δD toward cold regions. Despite known limitations due to temporal changes in intermittency of precipitation (Casado et al., 2020), vapor origin and transport (Helsen et al., 2006), sea ice extent (Noone, 2004), changes in condensation vs surface temperatures (Buizert et al., 2021) or deposition and post-deposition effects (Casado et al., 2018), the spatial relationship between surface temperature and surface snow δD and $\delta^{18}O$ has long been used to establish an isotopic paleothermometer to infer past temperature variations at least qualitatively (Jouzel et al., 2013).

Today, the oldest continuous isotopic record from ice cores has been retrieved at the Dome C through the European Project for Ice Coring Antarctica (EPICA) Dome C ice core (EDC) covering the last 800,000 years (800 kyrs) (Jouzel et al., 2007). The first analyses of water isotopic composition (δD) over the EDC ice core were performed at ~4 m resolution unveiling δD variations over 8 glacial - interglacial cycles (EPICA community members, 2004). Several years later, measurements of δD on bag samples (continuous 55 cm pieces of the EDC ice core) evidenced the millennial scale variability over the glacial periods in Antarctica (Jouzel et al., 2007; Stenni et al., 2010). In order to explore potential changes in high frequency variability in between different interglacial periods, Pol et al., (2010, 2011, 2014) used 11 cm resolution δD measurements over interglacial periods during Marine Isotopic Stages (MIS) 5, 11 and 19, i.e. the periods between 112 and 134 ka (kyrs before present), 392 and 427 ka, and 747 and 800 ka, respectively. Landais et al., (2015) focused on 11 cm resolution $\delta^{18}O$ over the last glacial period back to 60 ka.

Pol et al. (2014) used the high resolution water isotopic signals over MIS5 and 11 interglacial periods to estimate the relative variations of decadal to centennial climate variability during these interglacial periods with respect to the Holocene (Pol et al., 2011; 2014). Over the last glacial period, the high resolution $\delta^{18}O$ record showed an enhanced amplitude of the multi-decadal to centennial variability during the warm phases of the Antarctic Isotopic Maxima, or AIM (Landais et al., 2015). These AIM events are key climatic features of the last glacial period: they are counterparts of the Northern Hemisphere abrupt temperature increases first identified in the Greenland ice cores (Dansgaard et al., 1985; Blunier and Brook, 2001; EPICA community members, 2006).

High resolution water isotopic measurements over the EDC ice core are hence key to document the temporal patterns of climatic variability over the past 800 kyrs. Unfortunately, the analytical load to obtain the full 800 kyrs record at 11 cm resolution is enormous, and would represent 35,000 measurements. Even if several individual studies have been published, a complete synthesis of EDC high resolution δD and $\delta^{18}O$ records over the last 800 kyrs is still missing. This is an important limitation for the documentation of past changes in sub-orbital climatic variability in Antarctica and to compare the climatic variability features between glacial and interglacial periods or between different interglacial (glacial) periods. As an example, the interglacial periods before the Mid-Brunhes Transition (MBT, 430 ka) are cooler than the five most recent interglacial periods, but there is limited evidence available to document high resolution climate variability during interglacial periods before and after the MBT (Barth et al., 2018; Past Interglacials Working Group of PAGES, 2016). A first challenge is thus to provide homogeneous high resolution isotopic records.

A second challenge to characterize the past high frequency climate variability in Antarctica is non-temperature related variability in the water isotopes from the depositional process (Fischer et al., 1985; Laepple, 2018) and alteration and smoothing effects of post-deposition processes. Indeed, post-deposition processes (Casado et al., 2018, 2020; Steen-Larsen et al. 2014) and firn and ice diffusion (Gkinis et al., 2011, 2021) strongly limit the interpretation of water isotopic variability in term of climatic variability. In the case of old ice, the impact of diffusion which increases with depth and age can reach multi-centennial time scales and affect the climate variability recorded in $\delta^{18}O$ and δD. Pol et al. (2010) showed that the 11 cm resolution δD record of MIS 19 (3,147 – 3,190 m deep in the EDC ice core) was not bringing more information than the 55 cm resolution record due to large impact of diffusion at this depth of the core. This effect is particularly important to quantify for the 1.5 Ma ice core to be drilled in East Antarctica. Indeed, documenting the evolution of diffusion length with depth is key to anticipate what kind of information on climate variability can be retrieved from the deepest part of this future ice core.

Here we address the two aforementioned challenges (high-resolution records and influence of diffusion) by presenting a compilation of new high resolution measurements of $\delta^{18}O$ and δD on the EDC ice core. The first section presents the analytical methods used to perform high resolution measurements of δD and $\delta^{18}O$ of the different sections of the EDC ice core over the last decades as well as methods for spectral analyses and calculation of isotopic diffusion along the EDC ice core. The second section describes how the different measurements performed over the past 20 years in different institutes with different analytical methods can be compiled together into a single record. The third section uses the high resolution measurements to investigate changes in sub-orbital climatic variability across the last 800 kyrs and how diffusion can affect some of the observed features.

2. Materials and methods

2.1 The EPICA ice core

The Concordia Franco-Italian station is located at 3,233 m above sea level on the continental plateau of Antarctica, (75°06′12″S 123°21′30″E). The mean annual surface temperature is -54.5°C and the snow accumulation rate is ca. 25 mm water equivalent yr^{-1} (EPICA community members, 2004; Le Meur et al., 2018).

The EDC ice core has been drilled at the Concordia station on the Dome C where the ice flow was small (EPICA community members, 2004). The EDC drilling project started in 1996 and was completed in 2004. In 1999, a second ice core (EDC2) was drilled from the surface due to the drill for EDC1 being stuck at depth of 788 m. Bedrock was reached in 2004 at a depth of 3,190 m. From here onwards, we refer to EDC1 and EDC2 as the EDC ice core. By the time this second ice core was retrieved, the full 788 meters of EDC1 were analysed. Later, EDC2 measurements started 19 meters higher than the bottom end of the EDC1 ice core in order to have an overlap to reconnect the two cores without duplicating all the measurements on the common depth range.

After drilling and core logging, the EDC ice core was cut into 55 cm long sections and each section was further cut longitudinally on site for several measurements (e.g. water isotopes, physical properties, ^{10}Be, chemistry, and gas analysis). The archival piece (~ one quarter of the section) was stored in polystyrene boxes in the EPICA snow-cave at the Concordia station at -50°C. Two types of contiguous samples were dedicated for the analyses of water isotopes on the EDC ice core. First, a 55 cm long stick with a 1 cm^2 cross section was melted and stored on site in plastic bottles for the low resolution measurements. The second was a 55 cm length stick with a 2 cm^2 cross section that was cut into 11 cm length samples. Each sample was placed in a plastic sheath cut to obtain a plastic bag at the right dimension and then, the bag is thermally sealed. The sample is stored at -20°C during a few months prior to being melted and transferred into plastic bottles that were kept at -20°C.

2.2 Measurements techniques and coherency of the dataset

Several analytical techniques have been used to measure $\delta^{18}O$ and δD on the EDC1 and EDC2 ice cores (Tables 1 and 2). Initial analytical techniques included uranium reduction method for δD (Vaughn et al., 1988); CO_2 - H_2O equilibrium method for $\delta^{18}O$ (Myer et al., 2000); with the most recent method to determine $\delta^{18}O$ and δD on the EDC2 ice core using cavity ring down spectroscopy (CRDS) (Kerstel and Gianfrani, 2008; Busch and Busch, 1999). When uranium reduction has been replaced by CRDS measurements at LSCE, extensive series of comparison have been performed showing that there was an excellent agreement between the two methods within the uncertainty ranges of the instruments. The analytical precision for each method are comparable where 2σ values range between 1 and 1.4 ‰ for δD and between 0.1 and 0.4 ‰ for $\delta^{18}O$ (Table 2). Figure 1 displays the full high resolution (11 cm) datasets for $\delta^{18}O$ and δD of water over the EDC ice core.

2.3 Multi resolution analysis (MRA)

A discrete wavelet analysis is used to identify the contribution to the overall isotopic variability from signals of different periodicities (i.e. corresponding to decadal to multi-millennial signal variability). We produced a multi resolution analysis (MRA) using R software with the waveslim wavelet package (Whitcher, 2020) containing the MRA function with a Daubechies orthonormal wavelet filter. MRA is a mathematical analysis tool which decomposes a signal at different resolution levels. An important feature of MRA is its ability to capture temporally localised changes at its nearest neighbour. A low (high) resolution level corresponds to a coarse (detailed/high frequency) component of the original signal. Each MRA level can thus be used to interpret the temporal variability within a frequency range. Adding all MRA levels exactly reproduce the original undecomposed signal. As the wavelet analysis needs to be applied on time intervals with a uniform sample resolution, we divide the EDC isotopic record on the AICC2012 age scale (Bazin et al., 2013) into six intervals. These include the youngest interval between 0 and 56 ka (where the longest time span covered by 11 cm is 10 yr) to the bottom of the core with the oldest interval between 651 and 800 ka (where the longest time span covered by 11 cm is 320 yr) on the AICC2012 age scale (Bazin et al., 2013) (Table 3). Over each interval, we performed an interpolation with a uniform resolution corresponding to the

longest time span covered by 11 cm of ice (i.e. interpolation at 10 yr between 0 and 56 ka, 20 yr between 56 and 144 ka, see details for all periods on Table 3).

The resolution of the MRA for the different intervals was chosen to increase by a factor of two between two neighbouring intervals i and i+1, i being a number between 1 and 5. As a consequence, the 2nd MRA decomposition of the interval i has the same resolution than the 1st MRA of the interval i+1 (Table 3). We then concatenate the MRA with the same temporal resolution, leading to 9 successive composites (named a, b, c, d, e, f, g, h and i in table 3), the longest (composite f, g h and i) corresponding to the variability of the signal at a 320 yr resolution and covering the whole 800 ka and the shortest (composite a) corresponding to the variability of the signal at a 10 yr resolution and covering only the last 56 kyrs.

2.4 Effect of isotopic diffusion

The effect of isotopic diffusion with depth is convolved using a function G(z) of associated diffusion length σ_z (Gkinis, 2011; Laepple, 2018; Gkinis et al., 2021):

$$G(z) = \frac{1}{\sigma_z \sqrt{2\pi}} \exp\left(\frac{-z^2}{2\sigma_z^2}\right) \quad (1)$$

Where z is the depth along the ice core and σ_z is the diffusion length.

We quantify the amplitude decay of the signal between the initial amplitude A_0 and the measured amplitude A at a certain depth as described in Johnsen et al., (2000) and Gkinis et al., (2021) for given period λ with the following equation:

$$\frac{A}{A_0} = \exp\left(-2\left(\frac{\pi \times \sigma_z}{\lambda}\right)^2\right) \quad (2)$$

For our purpose, the diffusion length along the EDC ice core is calculated by considering the firn diffusion (i.e. due to water vapor diffusion in the open porosity) and the ice diffusion (i.e. due to water molecular diffusion in the ice matrix).

We used two different estimates for the firn diffusion length, σ_{firn}, along the EDC ice core. In a first approach, we assumed a constant σ_{firn} all along the EDC ice core and take the value of 0.07 m estimated by Johnsen et al. (2000) for EDC. In a second refined approach, we considered a changing σ_{firn} between interglacial and glacial periods as described in (Gkinis et al., 2021). This leads to a σ_{firn} varying between 0.075 m in interglacial period to 0.065 m in glacial period. The ice thinning, S, also affects the visible effect of firn diffusion length along the ice core so that the thinned firn diffusion length should be $\sigma_{thinned\_firn} = S \times \sigma_{firn}$. In this study, for consistency, we used the thinning function for the EDC ice core corresponding to the AICC2012 chronology (Bazin et al., 2013).

The ice diffusion depends on the thinning and the temperature. The following formulation permits to calculate the diffusion length associated with ice diffusion, σ_{ice}, as a function of age (and also depth) of the ice (Gkinis et al., 2011) :

$$\sigma_{ice}^2(\tau) = S(\tau)^2 \int_0^{\tau} 2D(t)S(t)^{-2}\, dt \quad (3)$$

With S the thinning of the ice layers at the considered age τ. In order to estimate the ice diffusion coefficient D(t), we use the classical formulation of Ramseier (1967):

$$D = D_0 \times \exp\left(\frac{-Q}{RT}\right) \quad (4)$$

with D_0 = 9.13 cm^2/s and Q = 59.820 kJ/mol. At -50°C, D is equal $8.866.10^{-14}$ cm^2/s and at -10°C, D is equal to $1.1993.10^{-11}$ cm^2/s, T represents the ice temperature from the borehole.

The total calculated diffusion length expected to be measured in the ice core is estimated using the diffusion length associated with the firn diffusion and the diffusion length associated with ice diffusion in a quadratic addition, so that:

$$\sigma_z = \sqrt{(\sigma_{ice}^2 + \sigma_{thinned\_firn}^2)} \quad (5)$$

The increase of the diffusion length for increasing depth in the ice core is shown in Figure S1. It is mainly due to the increase in temperature. The borehole temperature indeed evolves almost linearly from -53.5°C to -2.6°C along the 3,255 m ice core (Buizert et al., 2021). The variation of the calculated diffusion length around 3,000 m is explained by the variability of the thinning function (Dreyfus et al., 2007).

3. Coherency of different analytical measurements

Different analytical instruments and techniques have been used to determine $\delta^{18}O$ and δD in the EDC1 and EDC2 ice cores at different laboratories (Table 1). To determine the coherency of the different datasets, two different comparisons are performed; (1) comparison of the isotopic values from the same samples measured by different analytical techniques; and (2) comparison of the 55 cm sample resolution data with the 11 cm sample resolution data using a 5-point average. We averaged the 11 cm resolution on a 5-points window to compare it with the 55 cm resolution measurements on exactly the same window.

3.1 Comparison of isotopic data using different analytical techniques

The CRDS analysis in 2019-2020 measured previously analysed samples from 2004-2010: uranium reduction for δD on MIS 5.5 (1,670-1,693 m) and by H_2O-CO_2 equilibration for $\delta^{18}O$ (1,670-1,793 m) (Table 1). Figures 2 and 3 provide two examples of analyses performed on all overlapping intervals. Additional comparisons of isotopic data measured by different analytical techniques on the same samples are also presented in the supplementary material sections (Figures S5 and S6). The samples stayed refrozen between the different measurements and they have been refrozen immediately after analysis. Tests have been performed by storing low $\delta^{18}O$ and δD internal standards for several years in the freezer. In some cases, but not systematically and not significantly compared to the analytical precision, a small increase of $\delta^{18}O$ and δD could be obtained. In the comparison of the old and new record, we do not observe a systematic increase of $\delta^{18}O$ and δD for the samples analysed recently compared to the analyses performed 15 years ago so that we can unfortunately not give a solid explanation for the small differences between the series of measurements.

3.2 δD comparison

The difference between analytical techniques (Figure 2) seems to depend on the absolute value for δD (negative difference for low δD values). This is confirmed through a statistical test on the correlation between the absolute value of δD and the δD difference between the two series of measurements leading to a Pearson coefficient of 0.13 and a p-value of 0.003. Such an isotopic-dependent feature may arise from a possible calibration effect despite the fact that exchanges of internal laboratory water standards and regular intercalibrations were performed between the laboratories measuring water isotopes of the EDC ice cores.

Despite such tendency in the δD differences between the two series, the absolute value of the difference remains small. We use a Welch t-test to show that the 2010 and 2019 time series have equal means at a 99.9 % confidence level (t=3.5, N=1,000) with respect to the experimental margin of errors.

Finally, the distribution of the differences between the 2010 and the 2019 δD measurements is not Gaussian and not centred around 0 (Figure 2, panel c). Still, this distribution is narrow and is encompassed within a Gaussian distribution with 2σ = 1.4 ‰ associated with the classical analytical uncertainty of the δD measurements. Note that the analytical uncertainty associated with these CRDS measurements series has been evaluated from the analysis of the difference between the same samples (1,000 samples, which represent 10 % of the whole series) measured twice, 1 to 3 months apart. We thus conclude that the δD difference between the uranium reduction vs CRDS datasets is smaller than the uncertainty associated with CRDS measurements and thus that we can combine the different dataset if we consider a 2σ uncertainty of 1.4 ‰ on the final δD data.

3.3 $\delta^{18}O$ comparison

No significant statistical differences are observed between the $\delta^{18}O$ measurements performed using the CO_2-equilibrium and CRDS method. The standard deviation of the series of difference between 2010 and 2019 $\delta^{18}O$ measurements (2σ = 0.2 ‰) is smaller than the classical analytical uncertainty of the $\delta^{18}O$ measurements by CRDS (2σ = 0.4 ‰) (Figure 3). A statistical test was made on the correlation between the absolute value of $\delta^{18}O$ and the $\delta^{18}O$ difference between the two series of measurements leading to a Pearson coefficient of 0.0049 and a p-value of 0.9. In addition, we did a Welch t-test of the equality between two averages in $\delta^{18}O$ to know if the difference between the 2010 and 2019 $\delta^{18}O$ data is significantly different within the experimental margin of error. When doing so, the result shows that the two series have equal means at a 70 % confidence level (t=0.557, N=1,000).

Second, we compared low (55 cm) and high resolution (11 cm) $\delta^{18}O$ series after calculating the $\delta^{18}O$ average of five 11 cm samples that overlap with the same sample depth as the 55 cm samples (Figures S2 to S4). The difference between the two timeseries is 0.008 ± 0.001 ‰ (Figure S4). The comparison between low and high resolution series for δD was already

performed by (Pol et al., 2011, 2014). In the 2011 paper, the coherency between 55 cm and 11 cm samples was studied through the calculation of the average signal over five 11 cm data. They observed that the signal from the 55 cm samples is similar to the average signal with however a lower statistical accuracy (1σ = 0.5 ‰) than the average signal (1σ = 0. 23 ‰).

The two comparisons performed above suggest there is no signification statistical difference in the $\delta^{18}O$ and δD in the datasets compiled here (Figure 1).

4. Results and discussion

4.1 Recorded multi-decadal to multi-millenial isotopic variability over the last 800 kyrs

The compiled high resolution EDC water isotope record is presented in Figure 1. We applied the MRA decomposition on each of the 6 selected intervals (see Methods) and present decadal to multi-millennial variability across the last 800 kyrs (Figure 4). We calculated the running standard deviation (1σ) on a 3 kyrs window and we use this value as an estimate of the level of variability. For the first MRA composite at 10 yr resolution (a), we observe a stronger isotopic variability during the Holocene than during the Last Glacial Maximum (average 1σ of 0.46 ‰ and 0.24 ‰, respectively). The 20 yr variability (b) inferred from the second composite shows a globally uniform pattern over the last 150 kyrs. The 80 yr variability (d) is smaller during the interglacial periods (1σ=0.18 ‰) than during the glacial periods (1σ=0.30 ‰) over the last 400 kyrs. The 160 to 640 yr variability (e to g) also shows a small decrease of variability over interglacial periods and decreasing variability for the oldest ice core sections. For the lower frequency variabilities (composite at 1,280 and 2,560 yr resolution, h to i) the amplitude of the variability envelope increases during glacial inception and glacial period with a notable strong 2,560 yr variability at the onset of MIS 9 (1σ=1.13 ‰ compared to an average of 1σ=0.20 ‰ over the whole series). The large centennial to multi-centennial water isotope variability in glacial periods is linked to the succession of the Antarctic Isotopic Maxima (AIM) during glacial periods (EPICA community members, 2004; Jouzel et al., 2007). Finally, the decreasing amplitude of the signal variability toward older ages is probably the result of diffusion of water isotopes in firn open porosity and ice crystal. While we can disentangle the effect of diffusion and climate driven isotopic variability for low frequency signals and at greater depths, the respective influences of diffusion and climate are less obvious to identify at shallower depths and for high frequencies.

4.2 Effect of isotopic diffusion on the recorded signal variability

We evaluate the effects of diffusion on the isotopic signal recorded in ice core by computing the decrease of Holocene variability from equation (2). The calculated A/A_0 signal amplitude is hence scaled for each MRA composites to the mean amplitude of the variability of the MRA composite signal between 2 and 8 ka for each resolution (Figure 6).

As explained in the section “methods”, we used the ice diffusion coefficient from Ramseier (1967) with 2 different estimates for σ_{firn}. The different estimates of σ_{firn} do not have a significant effect on the calculated amplitude of the variability (Figure 5).

Diffusion has the expected effect to decrease the amplitude of the variability of the isotopic signal for older and deeper ice core sections (Figure 4). On the 10 yr series (a), diffusion dampens by half the amplitude of the recorded variability of the last glacial period compared to the Holocene. The calculated amplitude of the variability due to diffusion is actually much smaller than the recorded one which suggests that either the 10 yr isotopic variability during the last glacial period is larger than the 10 yr variability during the Holocene or that measurement noise is dominating the 10 yr variability.

For the deepest sections of the ice core, i.e. sections older than 600 ka, the diffusion model overestimates the damping of centennial and multi-centennial variability compared to what is retrieved from the ice core isotopic composition. This discrepancy calls for future reassessment of the isotopic diffusivity in the deepest sections of the EDC ice core.

4.3 Climate variability at different time intervals over the last 800 kyrs

Combining our high resolution water isotopic records with frequency analysis and the impact of diffusion, we can suggest some patterns for the decadal to millennial climate variability over the last 800 kyrs.

First, on decadal scale, our findings show a larger variability during the last glacial period compared to the Holocene. The analysis of (Jones et al., 2017) using water isotopic record on the WAIS Divide record in West Antarctica supports this higher variability at the decadal scale during the last glacial maximum. At the high accumulation site of WAIS, diffusion has minimal effect on the variability with a 4-15 yr periodicity and the higher water isotopic variability observed during this period is interpreted as an increase in the strength of the teleconnections between the tropical Pacific and West Antarctica (Jones et al., 2018). Jones et al. (2018) invoke the expansion of the Northern Hemisphere ice sheets during the LGM leading to a shift in the location of tropical convection to explain these characteristics. The same pattern is observed for the 20 yr periodicity (Figure 5, panel b), i.e. the calculated water isotopic diffused variability is smaller than the measured one during the last glacial period while there is a good agreement between the diffused and measured signal over MIS 5e. For the 40 and 320 yr periodicity (Figure 5, c to f), the variability of the last glacial period is also higher than the diffused Holocene variability. It is also the case for MIS 6 for the 80 yr periodicity (Figure 5, d) and MIS 8 and 10 for the 160 and 320 yr periodicity (Figure 5 e to f). For these periods and frequency ranges, the impact of diffusion on the variability is limited, and the isotopic signal in the ice core preserved. The multi-centennial variability increase during glacial periods can be related to the presence of AIM.

Our analysis shows that there is a clear enhanced isotopic variability during glacial periods at the multi-decadal to multi-centennial timescale in the EDC ice core which could be attributed to climate variability (Figure 4). This result is in agreement with the findings of Rehfeld et al. (2018) using a worldwide data synthesis showing increased interannual to millennial climatic variability during the last glacial maximum with respect to the Holocene at all latitudes with an increase of the variance by a factor of 2 in the high latitudes of the Southern Hemisphere, a result in agreement with output of coupled model simulations (Rehfeld et al., 2018).

Second, while the effect of diffusion is important when we want to compare variability from one interglacial periods to another, it does not affect the evolution of the recorded variability during the course of an interglacial period.

A previous study focused on the warm phase of MIS 5 (115.5 to 132 ka), where the wavelet analysis of the 11cm resolution δD record showed three different isotopic phases with different levels of variability (Pol et al., 2014). The first phase from 111 to 119 ka has a low orbital forcing context but the variability increases during the entry in glaciation, with centennial dominant periodicities. The second phase from 119 to 123 ka is a stable warm phase, warmer than the Holocene. The δD variability of the second phase is notably lower than the other phases, 3.7 ‰ compared to a 4.5 ‰ average. Finally, during the third phase there is again a higher variability with dominant multi centennial periodicities between 123 and 133 ka.

When doing a similar analysis with our MRA decomposition, we find similar variability of the high resolution signal (Figure 6 a), i.e. the maximum amplitude of the multi-decadal to multi-centennial variability of the signal is encountered over the optimum of MIS 5 (phase 3 in Pol et al.,(2014), between 125 and 131 ka) and toward end of this warm period (phase 1 of Pol et al., (2014)). The minimum amplitude of the multi-decadal to multi-centennial variability of the signal is encountered between 119 and 123 ka (phase 2 in Pol et al., (2014)) when the $\delta^{18}O$ and δD signals are on a plateau.

Thus, during MIS 5, multi-decadal to multi-centennial variability of the water isotopic signal can be interpreted as climate variability at these multi-decadal to multi-centennial timescales. It can be compared to the variability over the interglacial period of MIS 9 (~ between 325 and 338.5 ka) also characterized by a temperature optimum at its start. The amplitudes of the variability for the different MRA decompositions for the interglacial period of MIS 9 cannot be directly compared to ones over MIS 5 because of the effect of diffusion and thinning (see figure 5). However, in figure 6 b we observe the same pattern than for MIS5: higher amplitudes for the multi-decadal to multi-centennial variability are observed over the $\delta^{18}O$ optimum (333 – 338 ka) and at the end of this warm period (321 – 326 ka) while the minimum amplitudes for the multi-decadal to multi-centennial variability is observed over the plateau of the interglacial period (326 – 332 ka). This result strengthens the conclusion of Pol et al. (2014) that the climate over temperature optimum of interglacial periods may also be more variable at the multi-decadal to multi-centennial timescale. A parallel can be drawn with the larger high frequency water isotopic variability observed during temperature optimum of the AIM of the last glacial period on the EDC ice core (Landais et al., 2015) since this temperature optimum at the beginning of the interglacial could also be the result of millennial scale variability (Past Interglacials Working Group of PAGES, 2016).

5 Conclusion

Here, we compiled and presented a EDC ice core water isotopic record ($\delta^{18}O$ and δD) using new and previously published 11 cm data spanning the last 800 kyrs. This compilation and the comparison performed between different series of measurements showed that water isotopic data measured by different laboratories and techniques over the last 20 years on the same samples display no significant statistical difference and are within analytical uncertainty. As a result, all the available EDC water isotope data are combined to produce a continuous high resolution dataset at mostly 11 cm sample resolution.

A MRA decomposition of the water isotopic record at temporal resolution varying between 10 and 2,560 years shows that the variability during glacial periods at multi-decadal to multi-centennial time scales is higher than the variability during the Holocene and that the variability is enhanced over early temperature optimum during MIS 5 and 9. These results are not

influenced by diffusion in the firn open porosity and in the ice matrix, but the interpretation of high resolution δD and $\delta^{18}O$ profiles needs to take this effect into account. Finally, our study calls for further analyses for quantifying the diffusivity in EDC which is essential in the perspective of the Beyond EPICA-Oldest Ice core.

References

Barth, A. M., Clark, P. U., Bill, N. S., He, F., and Pisias, N. G.: Climate evolution across the Mid-Brunhes Transition, Clim. Past, 14, 2071–2087, https://doi.org/10.5194/cp-14-2071-2018, 2018.

Bazin, L., Landais, A., Lemieux-Dudon, B., Toyé Mahamadou Kele, H., Veres, D., Parrenin, F., Martinerie, P., Ritz, C., Capron, E., Lipenkov, V., Loutre, M.-F., Raynaud, D., Vinther, B., Svensson, A., Rasmussen, S. O., Severi, M., Blunier, T., Leuenberger, M., Fischer, H., Masson-Delmotte, V., Chappellaz, J., and Wolff, E.: An optimized multi-proxy, multi-site Antarctic ice and gas orbital chronology (AICC2012): 120–800 ka, Clim. Past, 9, 1715–1731, https://doi.org/10.5194/cp-9-1715-2013, 2013.

Bereiter, B., Eggleston, S., Schmitt, J., Nehrbass-Ahles, C., Stocker, T. F., Fischer, H., Kipfstuhl, S., and Chappellaz, J.: Revision of the EPICA Dome C CO_2 record from 800 to 600 kyr before present: Analytical bias in the EDC CO2 record, Geophys. Res. Lett., 42, 542–549, https://doi.org/10.1002/2014GL061957, 2015.

Blunier, T. and Brook, E. J.: Timing of Millennial-Scale Climate Change in Antarctica and Greenland During the Last Glacial Period, Science, 291, 109–112, https://doi.org/10.1126/science.291.5501.109, 2001.

Buizert C., Fudge T. J., Roberts W. H. G., Steig E. J., Sherriff-Tadano S., Ritz C., Lefebvre E., Edwards J., Kawamura K., Oyabu I., Motoyama H., Kahle E. C., Jones T. R., Abe-Ouchi A., Obase T., Martin C., Corr H., Severinghaus J. P., Beaudette R., Epifanio J. A., Brook E. J., Martin K., Chappellaz J., Aoki S., Nakazawa T., Sowers T. A., Alley R. B., Ahn J., Sigl M., Severi M., Dunbar N. W., Svensson A., Fegyveresi J. M., He C., Liu Z., Zhu J., Otto-Bliesner B. L., Lipenkov V.Y., Kageyama M., and Schwander J.: Antarctic surface temperature and elevation during the Last Glacial Maximum, Science, 372, 1097–1101, https://doi.org/10.1126/science.abd2897, 2021.

Busch, K. W. and Busch, M. A. (Eds.): Cavity-Ringdown Spectroscopy: An Ultratrace-Absorption Measurement Technique, American Chemical Society, Washington, DC, https://doi.org/10.1021/bk-1999-0720, 1999.

Casado, M., Landais, A., Picard, G., Münch, T., Laepple, T., Stenni, B., Dreossi, G., Ekaykin, A., Arnaud, L., Genthon, C., Touzeau, A., Masson-Delmotte, V., and Jouzel, J.: Archival processes of the water stable isotope signal in East Antarctic ice cores, The Cryosphere, 12, 1745–1766, https://doi.org/10.5194/tc-12-1745-2018, 2018.

Casado, M., Münch, T., and Laepple, T.: Climatic information archived in ice cores: impact of intermittency and diffusion on the recorded isotopic signal in Antarctica, Clim. Past, 16, 1581–1598, https://doi.org/10.5194/cp-16-1581-2020, 2020.

Dansgaard, W.: Greenland ice core studies. Paleogeography, Paleoclimatology, Paleoecology, 50: 185-187, 1985.

Dreyfus, Parrenin, F., Barnola, J-M., Beer, J., Blunier, T., Castellano, E.: The EDC3 chronology for the EPICA Dome C ice core. Climate of the Past Discussions, pp.575-606, 2007.

Ekaykin, A. A., Lipenkov, V. Ya., Barkov, N. I., Petit, J. R., and Masson-Delmotte, V.: Spatial and temporal variability in isotope composition of recent snow in the vicinity of Vostok station, Antarctica: implications for ice-core record interpretation, Ann. Glaciol., 35, 181–186, https://doi.org/10.3189/172756402781816726, 2002.

EPICA community members: Eight glacial cycles from an Antarctic ice core, Nature, 429, 623–628, https://doi.org/10.1038/nature02599, 2004.

Fisher D. A., Reeh, N., Clausen, H.B.: Stratigraphic noise in time series derived from ice cores. Annals of glaciology 7, 1985.

Gkinis, V., Ph.D. thesis, University of Copenhaguen, Center for Ice and Climate (2011): High resolution water isotope data from ice cores.

Gkinis, V., Popp, T. J., Blunier, T., Bigler, M., Schüpbach, S., and Johnsen, S. J.: Water isotopic ratios from a continuously melted ice core sample, Others (Wind, Precipitation, Temperature, etc.)/Laboratory Measurement/Instruments and Platforms, https://doi.org/10.5194/amtd-4-4073-2011, 2011.

Gkinis, V., Holme, C., Kahle, E. C., Stevens, M. C., Steig, E. J., and Vinther, B. M.: Numerical experiments on firn isotope diffusion with the Community Firn Model, J. Glaciol., 67, 450–472, https://doi.org/10.1017/jog.2021.1, 2021.

Gkinis, V.; Dahl-Jensen, D.; Steffensen, J. P.; Vinther, B. M.; Landais, A.; Jouzel, J.; Masson-Delmotte, V.; Cattani, O.; Minster, B.; Grisart, A.; Hörhold, M.; Stenni, B.; Selmo, E. (2021b): Oxygen-18 isotope ratios from the EPICA Dome C ice core at 11 cm resolution. PANGAEA, https://doi.org/10.1594/PANGAEA.939445

Helsen, M. M., van de Wal, R. S. W., van den Broeke, M. R., Masson-Delmotte, V., Meijer, H. A. J., Scheele, M. P., and Werner, M.: Modeling the isotopic composition of Antarctic snow using backward trajectories: Simulation of snow pit records, J. Geophys. Res., 111, D15109, https://doi.org/10.1029/2005JD006524, 2006.

Johnsen, Cuffey, K. M., Schwander, J., and Creyts, T.: Diffusion of stable isotopes in polar firn and ice : the isotope effect in firn diffusion, 21, 2000.

Jones, T. R., Cuffey, K. M., White, J. W. C., Steig, E. J., Buizert, C., Markle, B. R., McConnell, J. R., and Sigl, M.: Water isotope diffusion in the WAIS Divide ice core during the Holocene and last glacial, J. Geophys. Res. Earth Surf., 122, 290–309, https://doi.org/10.1002/2016JF003938, 2017.

Jones, T. R.; Roberts, W. H. G.; Steig, E. J.; Cuffey, K. M.; Markle, B. R.; White, J. W. C. (2018). Southern Hemisphere climate variability forced by Northern Hemisphere ice-sheet topography. Nature, (), –. doi:10.1038/nature24669

Jouzel, J., Masson-Delmotte, V., Cattani, O., Dreyfus, G., Falourd, S., Hoffmann, G., Minster, B., Nouet, J., Barnola, J. M., Chappellaz, J., Fischer, H., Gallet, J. C., Johnsen, S., Leuenberger, M., Loulergue, L., Luethi, D., Oerter, H., Parrenin, F., Raisbeck, G., Raynaud, D., Schilt, A., Schwander, J., Selmo, E., Souchez, R., Spahni, R., Stauffer, B., Steffensen, J. P., Stenni, B., Stocker, T. F., Tison, J. L., Werner, M., and Wolff, E. W.: Orbital and Millennial Antarctic Climate Variability over the Past 800,000 Years, Science, 317, 793–796, https://doi.org/10.1126/science.1141038, 2007.

Jouzel, J., Delaygue, G., Landais, A., Masson-Delmotte, V., Risi, C., and Vimeux, F.: Water isotopes as tools to document oceanic sources of precipitation: Water Isotopes and Precipitation Origin, Water Resour. Res., 49, 7469–7486, https://doi.org/10.1002/2013WR013508, 2013.

Kerstel, E. and Gianfrani, L.: Advances in laser-based isotope ratio measurements: selected applications, Appl. Phys. B, 92, 439–449, https://doi.org/10.1007/s00340-008-3128-x, 2008.

Laepple, T., Münch, T., Casado, M., Hoerhold, M., Landais, A. and Kipstuhl, S.: On the similarity and apparent cycles of isotopic variations in East Antarctic snow pits, Cryosphere 12(1), 169-187, doi:10.5194/tc-12-169-2018, 2018.

Landais, A., Masson-Delmotte, V., Stenni, B., Selmo, E., Roche, D. M., Jouzel, J., Lambert, F., Guillevic, M., Bazin, L., Arzel, O., Vinther, B., Gkinis, V., and Popp, T.: A review of the bipolar see–saw from synchronized and high resolution ice core water stable isotope records from Greenland and East Antarctica, Quat. Sci. Rev., 114, 18–32, https://doi.org/10.1016/j.quascirev.2015.01.031, 2015.

Landais, A., Stenni, B., Masson-Delmotte, V., Jouzel, J., Cauquoin, A., Fourré, E., Minster, B., Selmo, E., Extier, T., Werner, M., Vimeux, F., Uemura, R., Crotti, I., and Grisart, A.: Interglacial Antarctic–Southern Ocean climate decoupling due to moisture source area shifts, Nat. Geosci., 14, 918–923, https://doi.org/10.1038/s41561-021-00856-4, 2021.

Laskar, J., Robutel, P., Joutel, F., Gastineau, M., Correia, A. C. M., and Levrard, B.: A long-term numerical solution for the insolation quantities of the Earth, Astron. Astrophys., 428, 261–285, https://doi.org/10.1051/0004-6361:20041335, 2004.

Le Meur, E., Magand, O., Arnaud, L., Fily, M., Frezzotti, M., Cavitte, M., Mulvaney, R., and Urbini, S.: Spatial and temporal distributions of surface mass balance between Concordia and Vostok stations, Antarctica, from combined radar and ice core data: first results and detailed error analysis, The Cryosphere, 12, 1831–1850, https://doi.org/10.5194/tc-12-1831-2018, 2018.

Lüthi, D., Le Floch, M., Bereiter, B., Blunier, T., Barnola, J.-M., Siegenthaler, U., Raynaud, D., Jouzel, J., Fischer, H., Kawamura, K., and Stocker, T. F.: High-resolution carbon dioxide concentration record 650,000–800,000 years before present, Nature, 453, 379–382, https://doi.org/10.1038/nature06949, 2008.

Meyer, H., Schönicke, L., Wand, U., Hubberten, H. W., and Friedrichsen, H.: Isotope Studies of Hydrogen and Oxygen in Ground Ice - Experiences with the Equilibration Technique, Isotopes Environ. Health Stud., 36, 133–149, https://doi.org/10.1080/10256010008032939, 2000.

Noone, D.: Sea ice control of water isotope transport to Antarctica and implications for ice core interpretation, J. Geophys. Res., 109, D07105, https://doi.org/10.1029/2003JD004228, 2004.

Past Interglacials Working Group of PAGES: Interglacials of the last 800,000 years, Rev. Geophys., 54, 162–219, https://doi.org/10.1002/2015RG000482, 2016.

Pol, K., Masson-Delmotte, V., Johnsen, S., Bigler, M., Cattani, O., Durand, G., Falourd, S., Jouzel, J., Minster, B., and Parrenin, F.: New MIS 19 EPICA Dome C high resolution deuterium data: Hints for a problematic preservation of climate variability at sub-millennial scale in the “oldest ice,” Earth Planet. Sci. Lett., 298, 95–103, https://doi.org/10.1016/j.epsl.2010.07.030, 2010.

Pol, K., Debret, M., Masson-Delmotte, V., Capron, E., Cattani, O., Dreyfus, G., Falourd, S., Johnsen, S., Jouzel, J., Landais, A., Minster, B., and Stenni, B.: Links between MIS 11 millennial to sub-millennial climate variability and long term trends as revealed by new high resolution EPICA Dome C deuterium data – A comparison with the Holocene, Clim. Past, 7, 437–450, https://doi.org/10.5194/cp-7-437-2011, 2011.

Pol, K., Masson-Delmotte, V., Cattani, O., Debret, M., Falourd, S., Jouzel, J., Landais, A., Minster, B., Mudelsee, M., Schulz, M., and Stenni, B.: Climate variability features of the last interglacial in the East Antarctic EPICA Dome C ice core, Geophys. Res. Lett., 41, 4004–4012, https://doi.org/10.1002/2014GL059561, 2014.

Ramseier, R. O.: Self-diffusion of tritium in natural and synthetic ice monocrystals, Journal of applied physics 38, 2553 1967. doi: 10.1063/1.1709948

Rehfeld, K., Münch, T., Ho, S. L., and Laepple, T.: Global patterns of declining temperature variability from the Last Glacial Maximum to the Holocene, Nature, 554, 356–359, https://doi.org/10.1038/nature25454, 2018.

Stenni, B., Jouzel, J., Masson-Delmotte, V., Röthlisberger, R., Castellano, E., Cattani, O., Falourd, S., Johnsen, S. J., Longinelli, A., and Sachs, J. P.: A late-glacial high-resolution site and source temperature record derived from the EPICA Dome C isotope records (East Antarctica), Earth Planet. Sci. Lett., 217, 183–195, https://doi.org/10.1016/S0012-821X(03)00574-0, 2004.

Stenni, B., Masson-Delmotte, V., Selmo, E., Oerter, H., Meyer, H., Röthlisberger, R., Jouzel, J., Cattani, O., Falourd, S., Fischer, H., Hoffmann, G., Iacumin, P., Johnsen, S. J., Minster, B., and Udisti, R.: The deuterium excess records of EPICA

Dome C and Dronning Maud Land ice cores (East Antarctica), Quat. Sci. Rev., 29, 146–159, https://doi.org/10.1016/j.quascirev.2009.10.009, 2010.

Vaughn, B. H., White, J. W. C., Delmotte, M., Trolier, M., Cattani, O., and Stievenard, M.: An automated system for hydrogen isotope analysis of water, Chem. Geol., 152, 309–319, https://doi.org/10.1016/S0009-2541(98)00117-X, 1998.

Veres, D., Bazin, L., Landais, A., Toyé Mahamadou Kele, H., Lemieux-Dudon, B., Parrenin, F., Martinerie, P., Blayo, E., Blunier, T., Capron, E., Chappellaz, J., Rasmussen, S. O., Severi, M., Svensson, A., Vinther, B., and Wolff, E. W.: The Antarctic ice core chronology (AICC2012): an optimized multi-parameter and multi-site dating approach for the last 120 thousand years, Clim. Past, 9, 1733–1748, https://doi.org/10.5194/cp-9-1733-2013, 2013.

Whitcher, B., 2020: Package Waveslim, Basic wavelet routines for one-, two-, and three dimensional signal processing, version 1.8.2, License BSD_3_clause, CRAN.

Acknowledgement

This work is a contribution to the European Project for Ice Coring in Antarctica (EPICA), a joint European Science Foundation and European Commission scientific program, funded by the European Union and by national contributions from Belgium, Denmark, France, Germany, Italy, Netherlands, Norway, Sweden, Switzerland, and the United Kingdom. The main logistic support was provided by Institut Polaire Français Paul-Emile Victor and Programma Nazionale Ricerche in Antartide.

A.G. was supported by the European Research Council under the European Union Horizon 2020 Programme ERC ICORDA (817493). We would like to thank Nancy Bertler, Andrew Moy and an anonymous referee for their careful evaluation and thoughtful comments.

Figures

Place of measurements	Date	Age (kyrs)	Depth (m)	Resolution (m)	Method	2σ (‰)	Reference
LSCE	2010	112-134	1,489-1,756	0.11	Uranium reduction	1	(Pol et al., 2014)
	2002 - 2007	0-27 0-800	0-577 0-3,189	0.55			(Jouzel et al., 2001) (Jouzel et al., 2007)
	2011	392-427	2,694-2,779	0.11		1	(Pol et al., 2011)
	2010	747-801	3,146-3,189	0.11		1	(Pol et al., 2010)
	2019	127-128.5 129.2-133 133.8-138	1,670-1,693 1,704-1,748 1,756-1,782	0.11		1.4	This study
	2019	245-267	2,309-2,372	0.11	CRDS spectroscopy analyser	1.4	This study
	2019	451-542	2,799-2,913	0.11		1.4	This study
	2019 - 2020	450-802	2,772-3,035 3,044-3,190	0.55		1.4	(Landais et al., 2021)
	2021	235-245	2,253-2,308	0.11		1	This study

Table 1: Summary of available δD measurements on the EDC ice core and associated analytical methods. 2σ values come from instrumental measurement uncertainty as provided in the original studies.

Place of measurements	Date	Age (kyrs)	Depth (m)	Resolution (m)	Method	2σ (‰)	Reference
LSCE	2019	127-128.5 129.2-133 133.8-138	1,670-1,693 1,704-1,748 1,756-1,782	0.11	CRDS spectroscopy analyser	0.4	This study
	2019	245-267	2,309-2,372	0.11		0.4	This study
	2019	451-542	2,799-2,913	0.11		0.4	This study
	2019 - 2020	450-802	2,772-3,035 3,044-3,190	0.55		0.4	(Landais et al., 2021)
University of Copenhagen	2001 - 2010 2021	0-3 3-3.6 7-9 9.3-34.2 34.5-60 60-115 116-120 121-124 125-128 129-133 134-142 248-415 543-802	6.6-120 120-134 234-288 290-656 659-946 946-1,528 1,539-1,583 1,594-1,638 1,649-1,693 1,704-1,748 1,759-1,803 2,317-2,756 2,794-3,190	0.11	CO_2 equilibration	0.14	(Gkinis 2011) (Landais et al., 2015) (Gkinis et al. 2021 b)
University of Trieste University of Parma	2001 2004 2010 2021	0-27 0-44.8 0-140 0-800	0-590 0-787 0-1,790 0-3,190	0.55		0.2	(Stenni et al., 2001) (Stenni et al., 2004) (Stenni et al., 2010) (Landais et al., 2021)

465

Table 2: Summary of available $\delta^{18}O$ measurements on the EDC ice core and associated analytical methods. 2σ values come from instrumental measurement uncertainty as provided in the original studies.

Interval / Decom Positions	Interval 1 (0-56 ka)	Interval 2 (56 - 144 ka)	Interval 3 (144 - 305 ka)	Interval 4 (305 - 420 ka)	Interval 5 (420 - 651 ka)	Interval 6 (651 - 800 ka)
MRA 1	10 (a)	20 (b)	40 (c)	80 (d)	160 (e)	320 (f)
MRA 2	20 (b)	40 (c)	80 (d)	160 (e)	320 (f)	640 (g)
MRA 3	40 (c)	80 (d)	160 (e)	320 (f)	640 (g)	1280 (h)
MRA 4	80 (d)	160 (e)	320 (f)	640 (g)	1280 (h)	2560 (i)
MRA 5	160 (e)	320 (f)	640 (g)	1280 (h)	2560 (i)	
MRA 6	320 (f)	640 (g)	1280 (h)	2560 (i)		
MRA 7	640 (g)	1280 (h)	2560 (i)			
MRA 8	1280 (h)	2560 (i)				
MRA 9	2560 (i)					

470

Table 3: Time resolution (in year) of the different MRA decomposition for specific intervals (0-56, 56-144, 144-305, 305-420, 420-651, 651-800 ka). Letters a, b, c, d, e and f represent segments that have the same time resolution and can be combined.

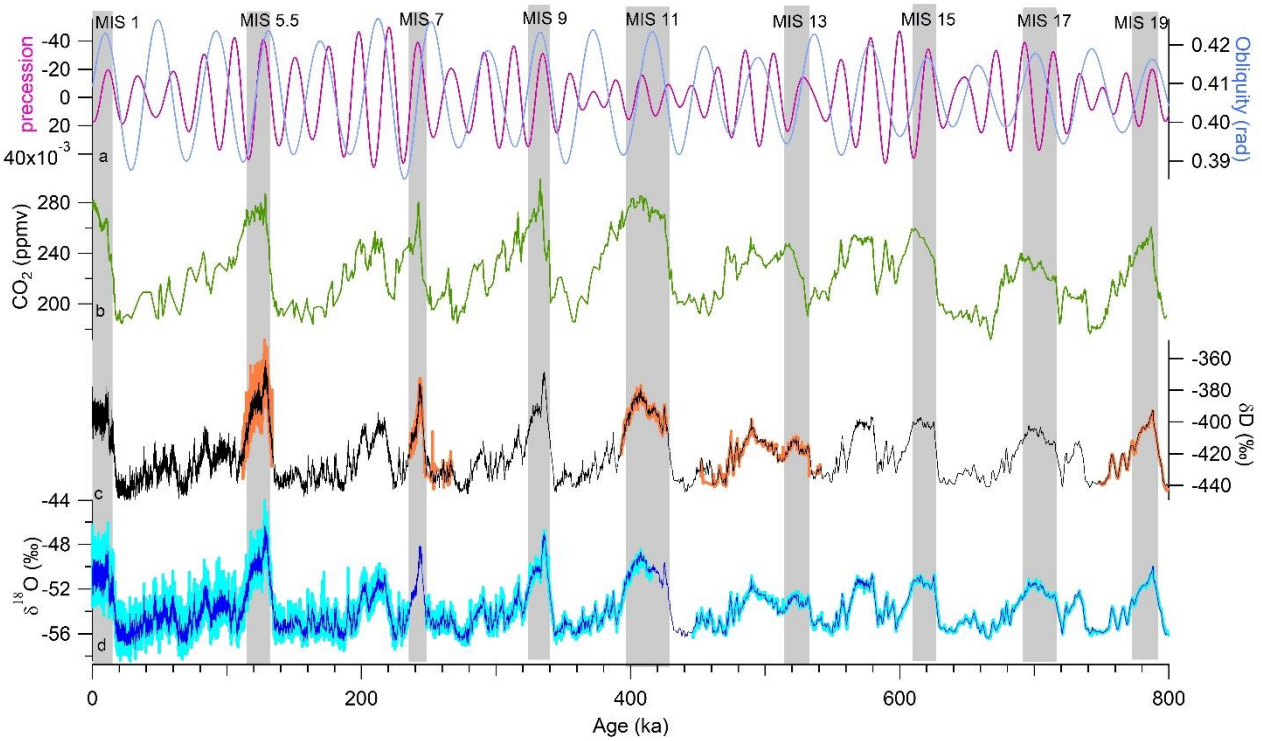

Figure 1: EDC ice core and other palaeoclimate records as well as variations in Milankovitch cycles over the past 800 kyrs. (a) precession (pink) and obliquity (blue) from Laskar et al., (2004); (b) Composite EDC and Vostok CO_2 record over the last 800 kyrs (Lüthi et al., 2008; Bereiter et al., 2015); (c) 11 cm (orange) and 55 cm resolution (black) of the EDC δD record; (d) 11 cm (light blue) and 55 cm resolution (dark blue) of the EDC $\delta^{18}O$ record. All ice core records are presented on the AICC2012 scale (Bazin et al., 2013; Veres et al., 2013). Grey rectangles indicate the position of interglacial periods.

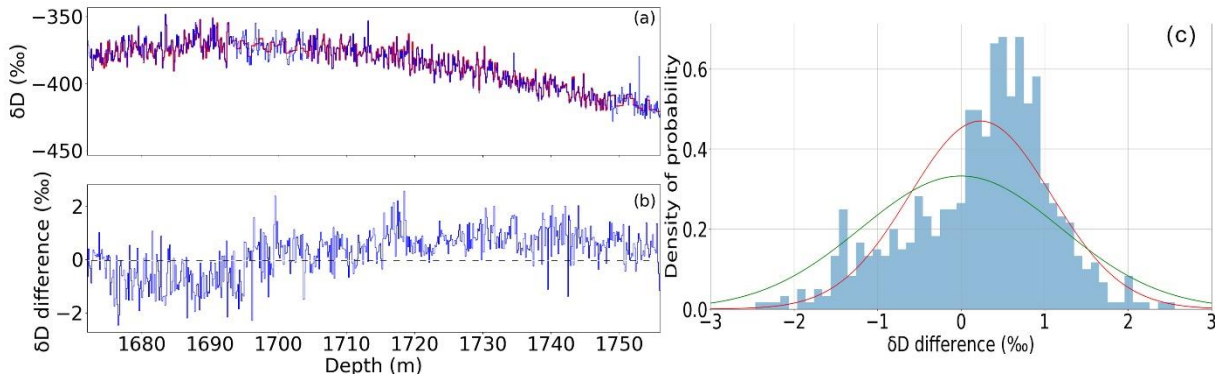

Figure 2: (a) EDC δD measurements versus depth (m) over Termination 2: in blue measurements completed in 2010 at LSCE (Uranium reduction method; Pol et al., 2014) and in red measurements completed in 2019 at LSCE (CRDS method). (b) Difference between the δD values measured in 2010 and 2019. (c) Probability Density Function for the difference between the first (Uranium reduction) and the new (CRDS) δD measurements. A Gaussian curve (red) is fitted to the data. A gaussian curve (green) is displayed with the standard deviation equal to the classically displayed 1σ uncertainty of δD measurements with CRDS method at LSCE (1σ = 0.7 ‰).

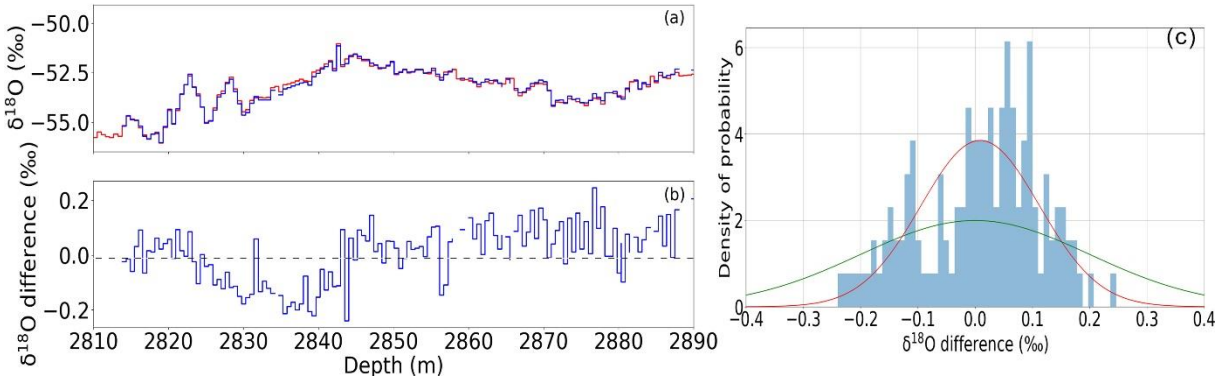

Figure 3: (a) EDC δ18O measurements versus depth (m) over Termination 6: in blue measurements completed in 2010 at the University of Triestre with CO_2 equilibration method and in red measurements completed in 2019 at LSCE (CRDS method). (b) Difference between the $\delta^{18}O$ values measured in 2010 and 2019. (c) Probability Density Function for the difference between the old (University of Triestre) and the new (LSCE) $\delta^{18}O$ measurements. A gaussian curve (red) is fitted to the data. A gaussian curve (green) is displayed with the standard deviation equal to the classically displayed 1σ uncertainty of $\delta^{18}O$ measurements by CRDS at LSCE (1σ = 0.2 ‰).

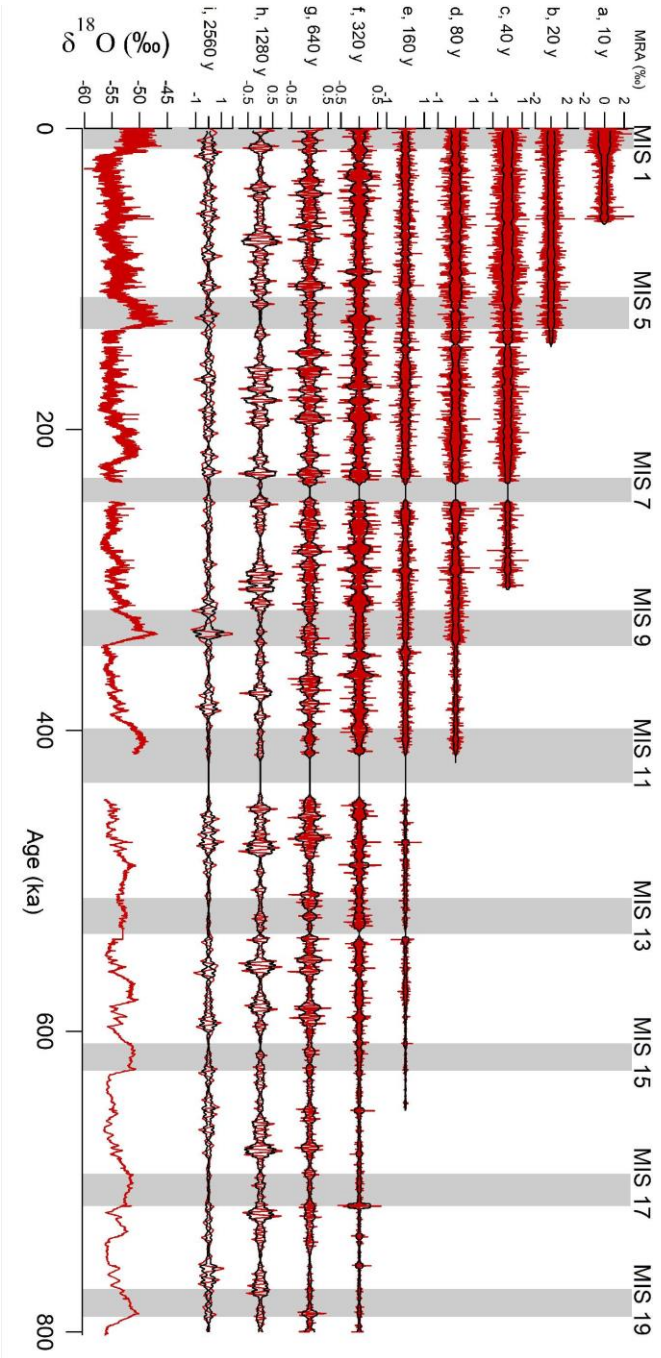

Figure 4: Contribution to the original $\delta^{18}O$ signal (red) of the MRA composites of resolution 10 (a), 20 (b), 40 (c), 80 (d), 160 (e), 320 (f), 640 (g), 1280 (h) and 2560 years (i). Marine Isotope Stage intervals are marked in grey bars. The black envelop presents the running standard deviation (1σ) on 3 kyr windows.

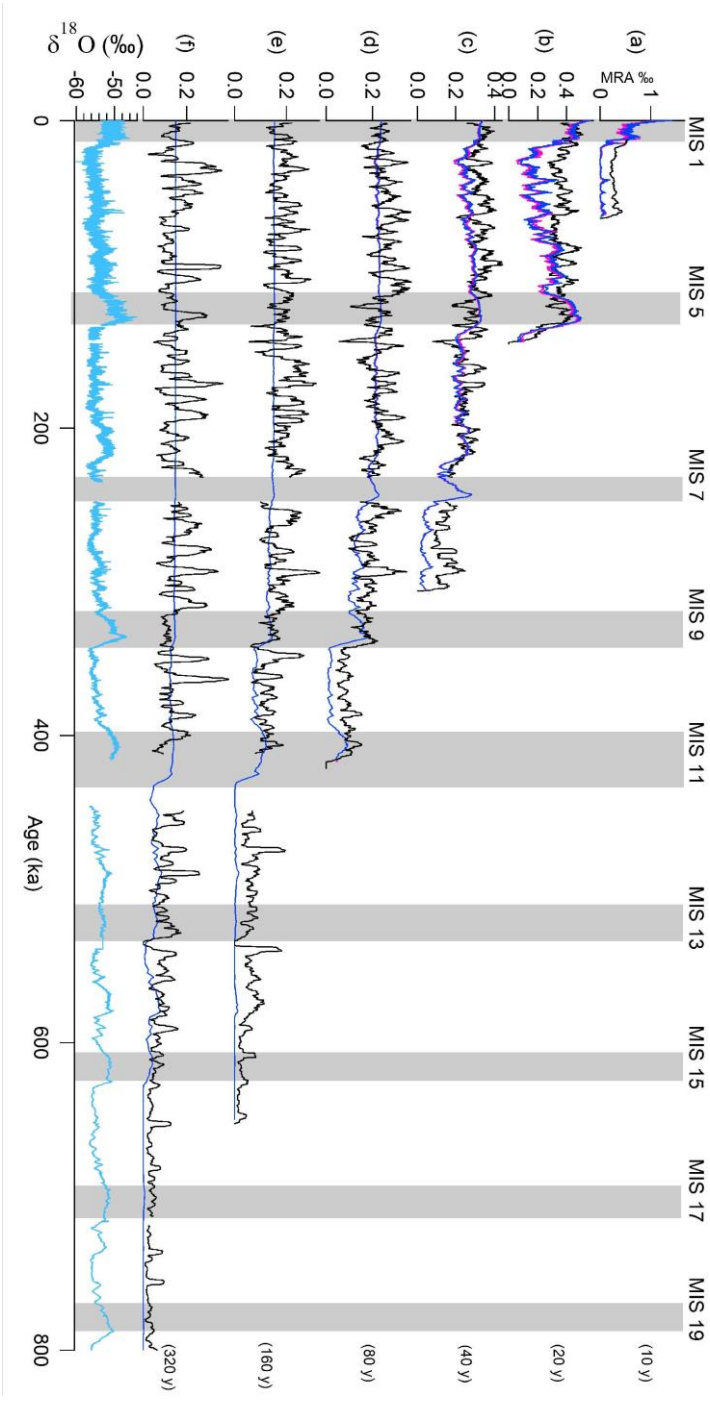

Figure 5: High resolution record (light blue) and comparison of its variability (3 ky standard deviation, black) to the variability (3 kyr standard deviation) of the diffused Holocene signal for the different periods (10, 20, 40, 80, 160, 320 years for panels (a) to (f)). The diffused Holocene signal has been calculated using two σ_{firn} estimates, one constant σ_{firn} of 7 cm (dark blue), and one variable σ_{firn} equal to 6.5 cm in glacial period and 7.5 cm in interglacial period (pink).

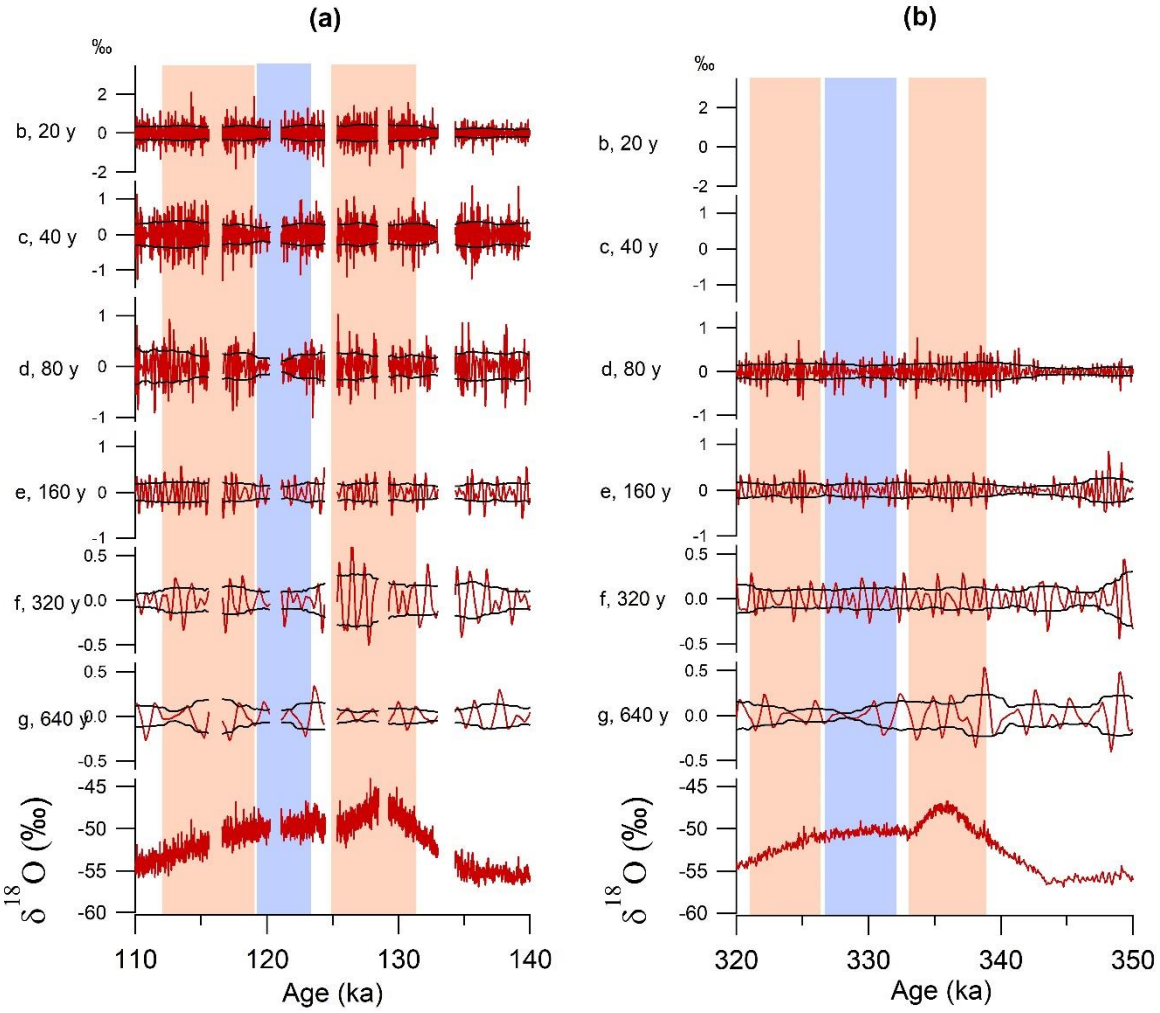

515 **Figure 6: Contribution to the original $\delta^{18}O$ signal (red) of the MRA composites of resolution 20 (b), 40 (c), 80 (d), 160 (e), 320 (f) and 640 (g) years (i) for MIS 5 (left - a) and MIS 9 (right - b). The black envelop presents the running standard deviation (1σ) on 3 kyr windows. The red rectangles indicate periods with enhanced variability and the blue rectangles indicate periods with reduced variability.**